Cite this as:
S. Nayak, P. U. Biedermann, M. Stratmann, A. Erbe: *Electrochimica Acta*, **106**, 472-482 (**2013**)

http://dx.doi.org/10.1016/j.electacta.2013.05.133

In situ infrared spectroscopic investigation of intermediates in the electrochemical oxygen reduction on n-Ge(100) in alkaline perchlorate and chloride electrolyte

Simantini Nayak[1], P. Ulrich Biedermann, Martin Stratmann[1], Andreas Erbe*
Max-Planck-Institut für Eisenforschung GmbH, Max-Planck-Str. 1, 40237, Düsseldorf, Germany

---

Abstract

For an understanding of the four electron transfer mechanism of the electrochemical oxygen reduction reaction (ORR), a direct detection of intermediates on well-defined working electrode surfaces is crucial, as it bridges the gap between electrochemistry and computation. Here, the ORR is studied on the crystalline semiconductor n-Ge(100) by electrochemical attenuated total reflection infrared (ATR-IR) spectroscopy in aqueous $NaClO_4$ and NaCl solutions at pH 10.5. Germanium-bound superoxide at a tilt angle of $\sim$45° with respect to the surface normal is found as an intermediate in both electrolytes. The frequency of the superoxide O–O stretching mode differs by 25 cm^{-1} between the two electrolytes, hinting at a complex formation between at least one of the anions and the superoxo-intermediate. This complex formation may be related to the different surface terminations of germanium in the two electrolytes. The surface concentration of the superoxide intermediate is proportional to the ORR current. Analysis of the relation between absorbance and current shows that the rate constant of the second electron transfer step in the ORR, i.e. the step from superoxide to peroxide, in NaCl is three times as high as in

---

*Corresponding author
Email address: `a.erbe@mpie.de`, `aerbe@arcor.de` (Andreas Erbe)
[1] ISE member.

$NaClO_4$.

Keywords: ATR-IR spectroscopy, oxygen reduction reaction, semiconductor, corrosion, kinetic analysis

---

1. Introduction

The electrochemical oxygen reduction reaction (ORR) involves the net transfer of 4 electrons and 4 protons to the O_2 molecule and is accompanied by the breaking of the formal double bond. The net reaction in alkaline solution is $O_2 + 4\,e^- + 2\,H_2O \longrightarrow 4\,OH^-$. As the ORR consists of several electron and proton transfer steps, the overall mechanism is rather complex. In some cases, H_2O_2 is formed as a product of an incomplete, two electron reduction, according to $O_2 + 2\,e^- + 2\,H_2O \longrightarrow H_2O_2 + 2\,OH^-$ [1, 2]. While interest in the ORR mechanism has witnessed a revival over the last decade, most contemporary work focuses on the ORR on noble metals, because of their use in fuel cell catalysts [3–7]. On the other hand, the ORR is crucial for corrosion processes as well, which typically occur on materials surfaces covered with semiconducting oxides [8]. In addition, alternatives to precious noble metals are highly desirable for fuel cells [9, 10].

Detailed electrochemical studies of the ORR involving materials relevant in industrial corrosion processes have been performed on corrosion-product covered Zn using a ring-disc electrode approach, and a route via H_2O_2 was found in alkaline solution [11]. Kinetic data is also available on Fe and steels [12, 13]. In all these cases, the oxide/electrolyte interface under study contains a semimetallic or semiconducting oxide, which is in contact with a bulk metal during the running ORR. No direct experimental information is available about the nature of species which directly reside on the electrode surface.

To that end, surface-sensitive vibrational spectroscopy can be used to detect reaction intermediates in situ and operando directly on the working electrode surface. It is particularly well-suited for studies of reaction intermediate's nature, as there is a direct relation between the vibrational frequencies of the intermediate's O–O stretching mode and the bond order: double bonds ($\sim$1550 cm^{-1}) as present in O_2, single bonds ($\sim$800 cm^{-1}) as present in peroxides including H_2O_2, and bonds with bond order 1.5 ($\sim$1200 cm^{-1}) present in superoxides can be clearly distinguished [14–16]. Furthermore, vibrational spectroscopy can be performed in situ under electrochemical conditions. Recent electrochemical studies on noble metals have been complemented by vibrational spectroscopic studies, which enable a detection of intermediates directly on the electrode surface [15, 17–23]. All of these studies use "surface-enhanced" spectroscopy or geometries involving small particles. It has the disadvantage that certain hotspots dominate the spectroscopic signal, which may not be representative for the surface states and electrochemical reactions on the electrode. Recent analyses of the electric fields in such surface enhanced studies show that some regions of the surface do not contribute at all to the resulting spectra [24, 25]. However, studies on flat metal surfaces with single reflection set-ups in external reflection geometry have been reported to yield very weak signals [26]. In principle, such a problem can be overcomed e.g. by using multiple-reflection internal reflection spectroscopy [16]. Several studies on oxygen surface species have been performed in contact with gas phases [27, 28], i.e. not under conditions of aqueous electrochemistry. Likewise, most computational studies, which yield quite detailed insights into adsorption sites, bonding situation and conformation of adsorbed molecules [21, 29, 30], are still far from conditions of aqueous electrochemical experiments.

In a recent study, the authors used n-doped Ge(100), a simple crystalline semiconductor, as a model surface to combine electrochemical, spectroscopic and computational studies of the ORR in $HClO_4$ [16]. The electrochemical properties of Ge are well characterised [31–33], and it has been proposed as a model for semiconducting passive films [34]. In acidic solution, a surface transition is observed to a fully H–terminated surface at low potentials [35–38]. This transition has been related to the onset of the ORR, as it involves a radical surface state [16, 36, 39, 40]. The previous study has detected superoxide and peroxide in situ and operando as intermediates in the ORR, and their orientation with respect to the surface has been determined to be mainly upright [16].

The current work presents an extension of the previous study to alkaline pH, which is directly relevant in oxygen corrosion. Attenuated total reflection infrared (ATR-IR) spectroscopy coupled to electrochemical experiments on a n-doped Ge(100) working electrode is used to analyse the intermediates during the ORR in two different electrolytes, $NaClO_4$ and NaCl at pH 10.5. Furthermore, a simple kinetic scheme is used to derive the relation between a surface concentration of an intermediate and the observed current.

2. Experimental

2.1. Spectro-electrochemical cell and experiments

Details of the experimental setup have been presented elsewhere [16]. Briefly, on the optical base of a SpectraTech Model 0001-100 horizontal ATR unit, a home-made cell has been placed. In this cell, trapezoidal Sb-doped n-type Ge(100) ATR prisms (Crystaltechno, Moscow, Russia; resistivity 10-40 Ω cm; size 52 mm · 20 mm · 0.5 mm; angle of incidence 60°) act as working electrode and have been placed on a copper base plate, which is insulated with a PTFE piece against the base. A PTFE reservoir for electrolyte was placed on top of the Ge crystal and sealed with FPM O-rings. The PTFE lid of the cell contains bores to hold a Ag/AgCl/3M KCl microreference electrode MI-403 (Microelectrodes Inc., Bedford, NH, USA), a Pt wire (Goodfellow, Huntingdon, UK) counter electrode, a gas inlet and outlet, as well as a liquid inlet. The sides of the PTFE liquid reservoir contain two additional liquid outlets. The cell assembly was placed in a Fourier transform IR spectrometer Biorad FTS3000 (Agilent Technologies) to record the ATR-IR spectra. Spectra were recorded with a liquid nitrogen cooled mercury cadmium telluride (MCT) detector in s- and p-polarisation. The spectral resolution was set to 4 cm^{-1} and 1000 interferograms were added for each spectrum. The results are displayed as absorbance A at a certain potential. For the calculation of A, the single channel spectrum R_{sample} at that potential was divided by a reference spectrum (R_{ref}),

$$A = -\log_{10}\left(\frac{R_{\text{sample}}}{R_{\text{ref}}}\right) \tag{1}$$

Spectra were taken in potential intervals of 50 mV. For all displayed absorbance spectra, R_{ref} was recorded at the initial potential of -0.29 V vs. SHE (unless noted otherwise). Final spectra were baseline corrected before further analysis. Baseline correction for quantification was performed for each peak individually. On both sides of the peak, were no peak-like absorption feature was visible in the spectrum, a certain interval of points was chosen. These points were fit to a polynomial of third or fourth order. The polynomial was then subtracted from the spectra. Details are described elsewhere [41]. Programs and further information are available on the internet [42]. For display over a larger spectral range, baseline correction was performed manually. Two points were placed at the beginning and the end of the interval under consideration, mostly 1500 and 900 cm^{-1}. Further, typically 18 points were placed within the interval. The majority of these points were distributed in regions were no peak was present, and few points were placed by eye under the peak to connect the points on either side. No spectra was considered for further analysis if a difference was observed in peak shape between the automatically baseline corrected and the manually baseline corrected spectrum. Likewise, spectra were discarded which showed otherwise a strong difference between manual and automatic baseline correction.

Analysis of the spectra in s- and p-polarisation proceeds in the same fashion as explained elsewhere [16]. The dichroic ratio $D = A_{\text{p}}/A_{\text{s}}$ (A_{p} - integrated absorbance of respective band in p-polarisation, A_s - integrated absorbance of respective band in s-polarisation) was used to determine the orientation of the transition dipole moment (TDM) of different species with respect to the surface normal [43, 44]. The orientational order parameter S_2 has been determined from the experimental D using $D = \frac{I_{0x}}{I_{0y}} + \frac{I_{0z}}{I_{0y}} \cdot \left(1 + \frac{3S_2}{1-S_2}\right)$ [44]. The squared amplitudes of the electric field components at the interface I_{0x}, I_{0y} and I_{0z} are calculated from the parameters of the experimental system [44, 45]. The right-handed Cartesian coordinate system is used where the ATR internal reflection element's surface normal points to the $-z$ direction, and the x direction is the projection of the direction of propagation onto the internal reflection element's surface [44].

S_2 is related to the angle θ between TDM and surface normal as $S_2 = \frac{3\langle\cos^2(\theta)\rangle - 1}{2}$ [44]. In all cases, only a single orientation has been assumed in the orientation distribution function of each TDM. A random orientation resulting in 54.6° is expected for dissolved or weakly physisorbed species [44].

The equations in the previous two paragraphs show that the absorbance in both polarisations is affected by the orientation. To obtain an absorbance which is proportional to the surface concentration, the effect of orientation on the absorbance needs to be excluded. Therefore, a field-weighted, orientation-independent integrated absorbance A_{iso} was obtained from A_p and A_s [16, 46]. This quantity is given as [46]

$$A_{iso} = A_s \cdot \left(2 - \frac{I_{0x}}{I_{0z}}\right) + A_p \cdot \frac{I_{0y}}{I_{0z}}. \tag{2}$$

Currents were recorded simultaneously with the measurement of IR spectra using the chronoamperometry mode of the potentiostat Ivimstat XR (Ivium, The Netherlands). Electrolytes were saturated with O_2 or Ar by purging the solution prior to experiments. During experiments, the gas volume above the electrolyte was continuously purged with O_2 or Ar. Before electrochemical ATR-IR experiments, cyclic voltammograms (CVs) were recorded. Results of the electrochemical experiments display the current density j, normalised to the surface area of the Ge in contact with electrolyte. The p*H* of 10.5 has been chosen because no surface roughening was observed in the experiments. All electrode potentials E are given with reference to the standard hydrogen electrode (SHE). All experiments were carried out at ambient temperature of $(23 \pm 2)°\mathrm{C}$.

2.2. Chemicals and cleaning of the Ge(100) electrode

For cleaning of Ge(100), several published protocols have been tested [32, 35, 36], which all lead to surface roughening. Therefore, the crystals were cleaned by dipping them into neutral Extran lab detergent (VWR) for 1 h, rinsing with ultrapure water extensively, and leaving them in 2-propanol for 1 h. The crystals were subsequently rinsed with excessive amounts of ultrapure water and dried under a N_2 stream prior to experiments. The final cleaning was performed by electrochemical oxidation of the species inside the spectro-electrochemical cell prior to experiments. At least four cycles from 0 V to -0.8 V were performed. The shape of cyclic voltammograms (CVs) and the absence of CH stretching modes in the subsequently recorded IR spectra indicate the successful cleaning of the Ge surface.

The electrolytes used in this work were 0.1 M $NaClO_4$ (VWR) and 0.1 M NaCl (VWR) in ultrapure water. The p*H* was adjusted to 10.5 by addition of 1 M aqueous NaOH (VWR).

2.3. Experiments with isotope labelled compounds

To verify band assignments, experiments with isotope labelled electrolyte and isotope labelled O_2 have been performed. First, experiments with electrolytes based on D_2O (VWR) were carried out. Electrolytes were prepared by dissolving the respective salt in D_2O. To adjust the basicity of the electrolytes, 1 M NaOD (Sigma-Aldrich) solution was added in the same amount as NaOH was added to the H_2O-based electrolytes. Second, experiments in H_2O in the presence of $^{18}O_2$ (Sigma-Alrich) were carried out. In this case, the electrolyte was saturated first with Ar. A portion of Ar-saturated electrolyte in a three-neck-flask was then purged with $^{18}O_2$, and subsequently pumped into the cell, using a peristaltic pump. CV measurements served as indicator that the cell was O_2-free initially, and that O_2 was present after electrolyte exchange.

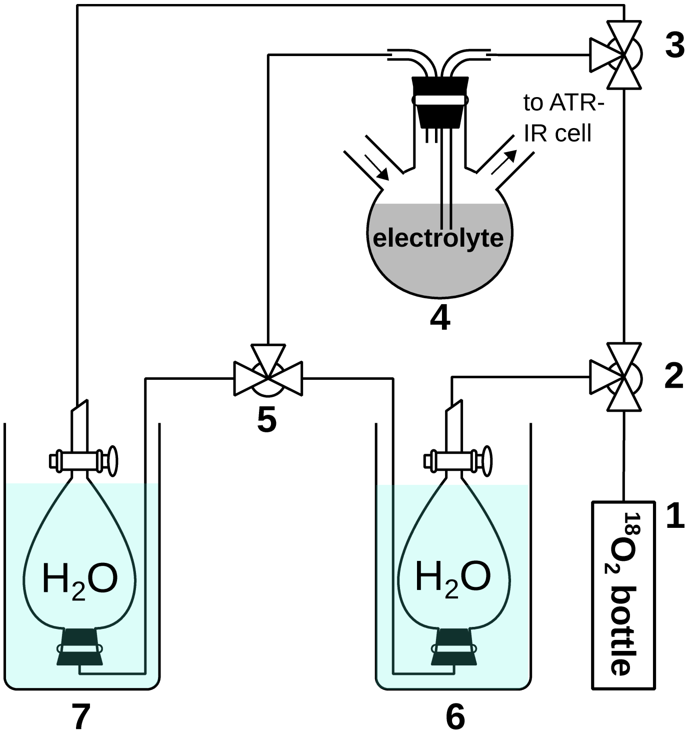

Figure 1 Simplified schematic drawing of the setup for purging the electrolyte with $^{18}O_2$. Function see text. **1** - gas cylinder with $^{18}O_2$. **2**,**3** and **5** - three way cocks. **4** - three neck flask with electrolyte which is purged. **6**, **7** - separation funnel in bucket with water.

The purging with $^{18}O_2$ was conducted in the following way (see Fig. 1). Two 500 mL glass separation funnels were placed upside down in a 10 L bucket each (**6**, **7**). These buckets were filled with deionized water, which was purged with N_2 during the experiments. The stoppers normally placed on top of the separation funnels were replaced by modified stoppers with two bores each. One bore was used as a feed-through to channel silicone tubing inside the separation funnel, the other bore was used to allow exchange of the liquid inside. The stopcock-sides of the two separation funnels were connected by silicone tubing to a three way cock (**3**); the third connection of this three way cock lead to the gas inlet of the three neck flask (**4**) containing the electrolyte to be purged. In that way, either of the two separation funnels could be switched to supply the gas which purged the electrolyte. The gas outlet of the three neck flask with electrolyte was connected to another three way cock (**5**). The two other connections from this second three way cock had tubing leading through the modified stopper into the separation funnels. Through the second three way cock, gas was channelled into the separation funnel which was not acting as a gas source in the current run, therefore acting as a gas collector. All connections were kept as short as possible, and were extensively purged with Ar before any experiment.

For the actual experiments, the two separation funnels were filled with water prior to purging with $^{18}O_2$. $^{18}O_2$ was then introduced into the system through a further three way cock (**2**) in one of the pipes leading to the electrolyte-containing flask gas inlet. After passing the electrolyte, the gas was collected in a separation funnel, where it replaced the water. After a sufficient amount of $^{18}O_2$ was collected, the $^{18}O_2$ source was removed from the setup (and three way cock **2** was set to allow a direct gas flow from separation funnel in **6** to **3**). The three way cocks were set such that the separation funnel containing $^{18}O_2$ was now becoming the source, while the second separation funnel was set to collect the $^{18}O_2$. Subsequently, a hydrostatic pressure was built up by pressing the $^{18}O_2$-containing separation funnel into the water, and lifting the water containing separation funnel out of the water. When all the gas had left the first separation funnel, and gas was present in the second separation funnel, the three way cocks were used again to switch the roles of gas source and gas collector between the two separation funnels. This procedure was repeated for 20-30 min to ensure repeated exposure of sufficient amounts of the electrolyte to $^{18}O_2$.

3. Results

3.1. ORR in 0.1 M $NaClO_4$ at p*H* 10.5

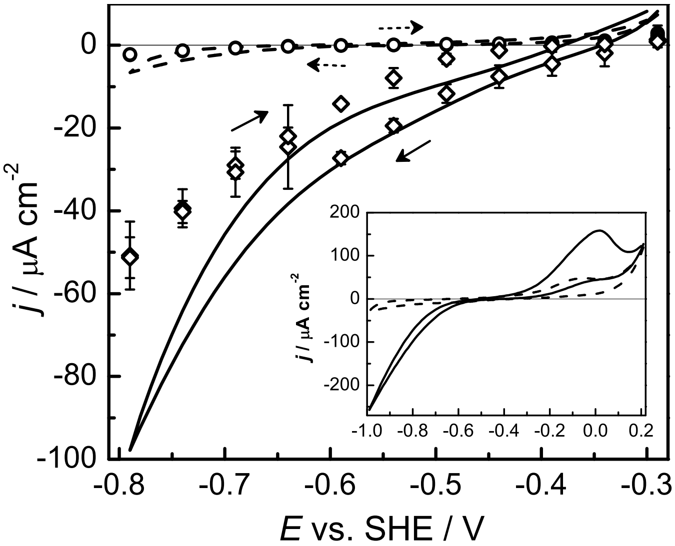

Figure 2 CVs in 0.1 M $NaClO_4$ (p*H* 10.5) on n-Ge(100) in electrolytes saturated with O_2 (—) and Ar (---). Time-averaged current densities during ATR-IR experiment are shown in O_2 (◇) and Ar (○) (respective spectra are shown in Fig. 3). The error bars represent the standard deviation during the experiment. Inset: CVs in O_2 and Ar over larger potential range. Horizontal lines indicate $j = 0$. Scan rate: 50 mV s^{-1}.

Fig. 2 shows CVs recorded in 0.1 M $NaClO_4$ at p*H* 10.5 in Ar and O_2 saturated electrolytes. An anodic peak is observed around 0 V. In Ar atmosphere, net cathodic currents are observed below -0.6 V, attributed to H_2 evolution. Scanning in negative direction in the presence of O_2 shows increased currents compared to Ar, which is a clear sign of a contribution of ORR to the overall currents. In O_2 saturated solution, ORR starts below -0.35 V in scans in negative direction. The time-averaged current densities measured while applying constant potentials during the ATR-IR experiment are also shown in Fig. 2 and follow the same trends as the CVs. Spectra from the same experiment are shown in Fig. 3.

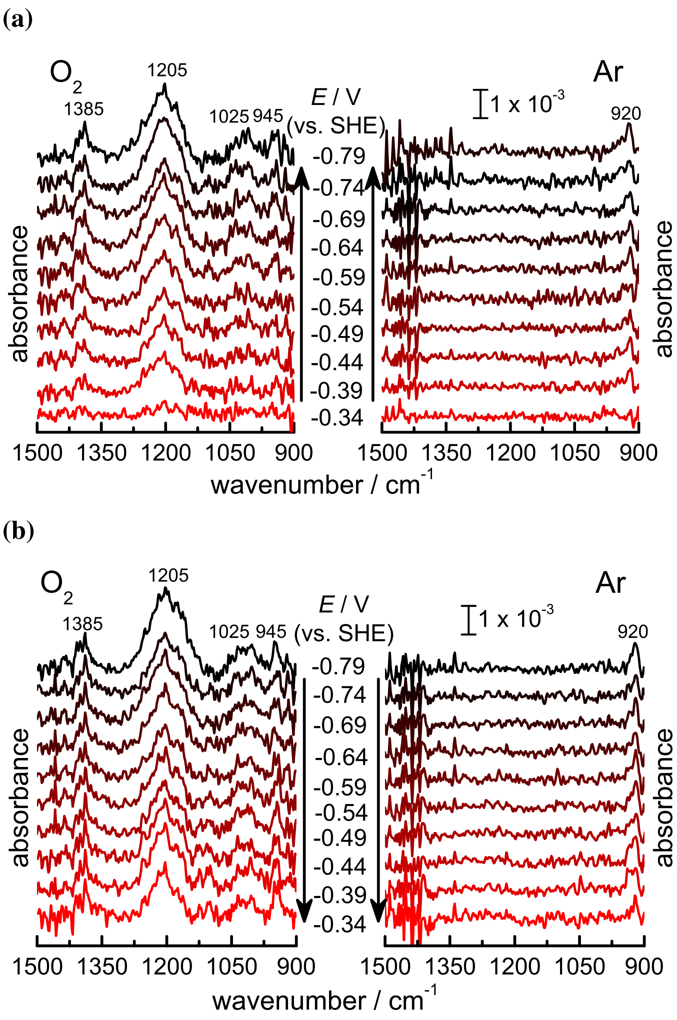

Figure 3 ATR-IR spectra recorded with p-polarisation in O_2 (left) and Ar (right) saturated 0.1 M $NaClO_4$ at p*H* 10.5 on n-Ge(100) with potential changing in (a) negative direction and (b) positive direction. Corresponding current densities are displayed in Fig. 2.

Fig. 3 shows a series of ATR-IR spectra, recorded at the indicated electrode potentials, in Ar and O_2 saturated solutions. In O_2-saturated solution, 4 peaks centered at $\sim$940 cm^{-1}, $\sim$1020 cm^{-1}, $\sim$1205 cm^{-1} and $\sim$1385 cm^{-1} are visible in the spectra. The most prominent peak at $\sim$1205 cm^{-1} is observed upon the onset of the ORR current at -0.39 V for the first time, grows with decreasing potentials (Fig. 3a) and decreases with increasing potentials (Fig. 3b). In the control experiment under Ar, it is not observed. Therefore, it is closely related to ORR. The same behaviour is observed for the modes at 1020 cm^{-1} and 1385 cm^{-1}). In the absence of O_2, only the weakest band is observed, shifted here to $\sim$920 cm^{-1} also increasing in absorbance with decreasing potentials. Therefore, this mode is not ORR related. No Ge–H stretching modes around 2000 cm^{-1} are observed in any of the experiments here.

The field-weighted integrated absorbance A_{iso}, which is proportional to the time-averaged surface coverage, was calculated for the absorptions at 1205 cm^{-1} and 1385 cm^{-1}, and is shown in Fig. 4. A_{iso} is compared to the time-averaged ORR current densities $j_{\text{ORR}} = j_{\text{O}_2} - j_{\text{Ar}}$ measured during the ATR-IR experiment. In order to consider only current due to ORR and to exclude the current originating from the hydrogen evolution reaction (HER), the experimental time-averaged current densities j_{Ar} in Ar measured during ATR-IR experiments were subtracted from the experimental time-averaged current densities j_{O_2} observed in O_2 during ATR-IR experiments. For both peaks shown in Fig. 4, A_{iso} is increasing with decreasing potential, as is j_{ORR}. In the reverse scan, the absorbance of the respective mode decreases with increasing potential, without returning to the initial absorbance. On the other hand, j_{ORR} reaches almost its initial value.

3.2. ORR in 0.1 M NaCl at p*H* 10.5

Fig. 5 shows the CVs recorded in 0.1 M NaCl at p*H* 10.5 in Ar and O_2 saturated electrolytes. Oxidation of the Ge surface is observed at +0.1 V. As in the case of $NaClO_4$ electrolyte, the currents during scans in cathodic direction are significantly higher in O_2 compared to Ar, indicating that ORR is occurring. The CV in O_2-saturated electrolyte

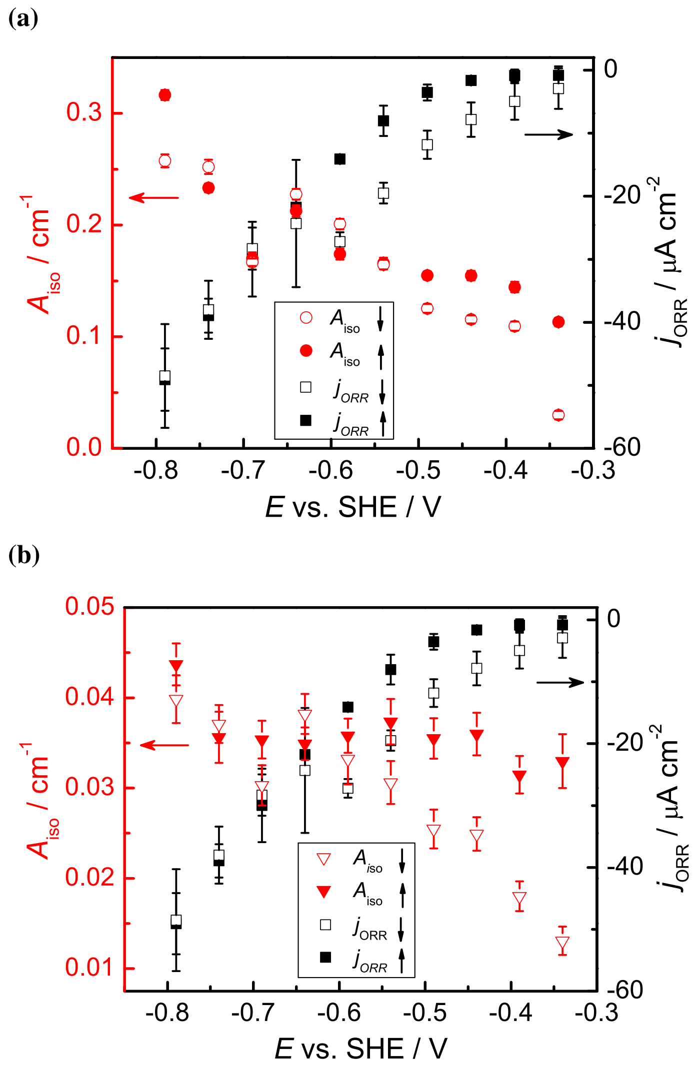

Figure 4 Potential dependence of A_{iso} of (a) the absorption at 1205 cm^{-1} and (b) the absorption at 1385 cm^{-1} in $NaClO_4$ at p*H* 10.5. For comparison, the current density due to ORR, j_{ORR} is also shown (right axis). Open symbols indicate scans with decreasing potential (↓), while filled symbols indicate scans with increasing potential (↑).

shows that ORR starts below -0.35 V. A full assignment of all waves in the CV is beyond the scope of this work. Fig. 5 also shows average current densities recorded during ac-

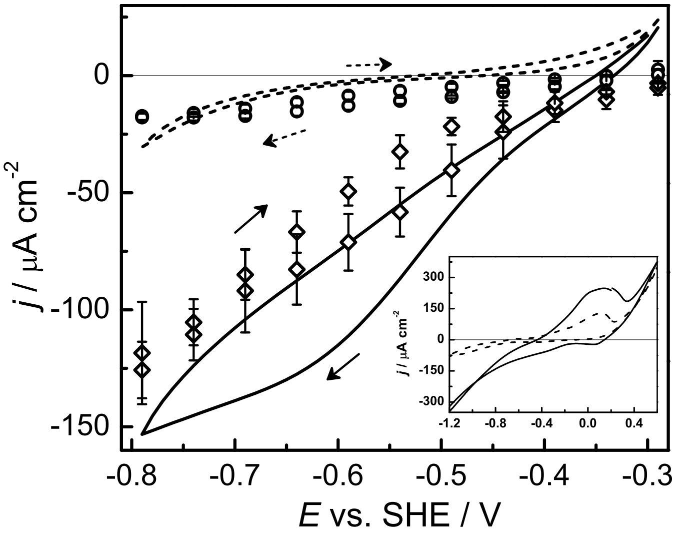

Figure 5 CV in 0.1 M NaCl at pH 10.5 on n-Ge(100) in O_2 (—) and Ar (---) atmosphere. Average current densities during ATR-IR experiment (Fig. 6) are shown in O_2 (◇) and Ar (○). Inset: CVs in O_2 and Ar over larger potential range. Horizontal lines indicate $j = 0$. Scan rate: 50 mV s^{-1}

.

quisition of ATR-IR spectra in O_2 and Ar-saturated electrolytes. Again, the substantially larger currents in O_2 show the occurrence of ORR. Compared to $NaClO_4$, the observed current densities are higher in NaCl.

ATR-IR experiments were carried out as described before, yielding spectra shown in Fig. 6. In Ar-saturated electrolyte, again only one peak is visible, here centred around ∼980 cm^{-1}. On the other hand, in O_2-saturated electrolytes, two broad bands are observed, in this case centred around ∼1230 cm^{-1} and ∼1390 cm^{-1}, the former with a shoulder on the low wavenumber side. The peak below 1000 cm^{-1} is also observed, centred at ∼960 cm^{-1}, with different shapes in the two different atmospheres.

Fig. 7 shows the potential dependence of A_{iso} of the absorptions at 1230 cm^{-1} and 1390 cm^{-1}, which are compared to j_{ORR} during the ATR-IR experiments. In both cases,

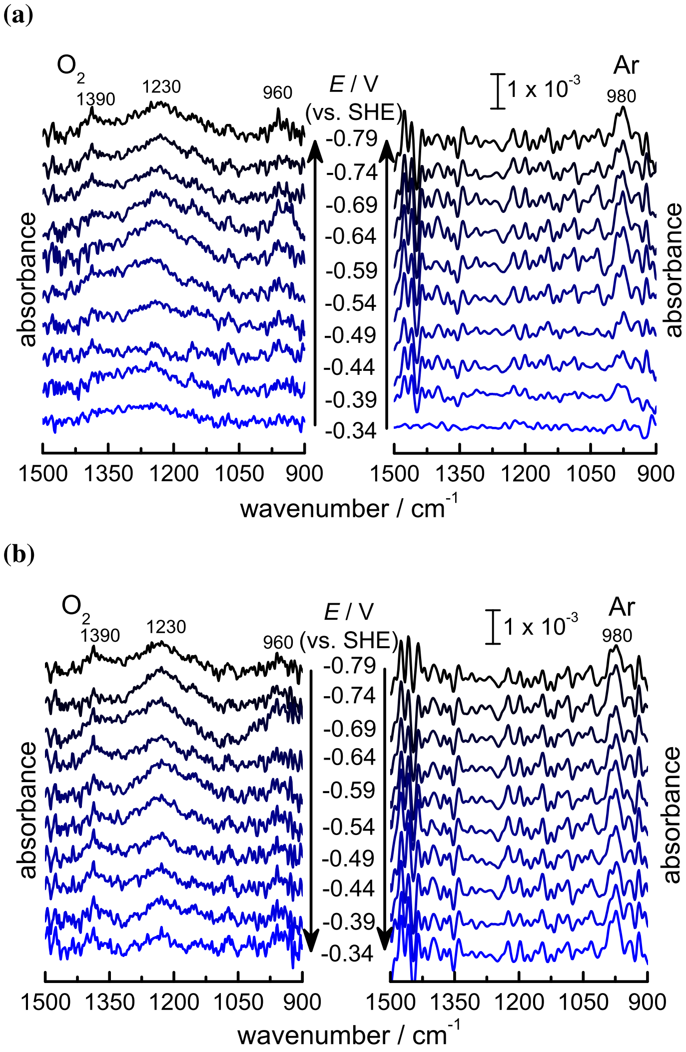

Figure 6 ATR-IR spectra with p-polarisation in O_2 (left) and Ar (right) saturated 0.1 M NaCl at p*H* 10.5 on n-Ge(100) in direction of (a) decreasing potential and (b) increasing potential. Corresponding j are displayed in Fig. 5.

the absorbance increases with decreasing potentials, following the trend in j_{ORR}. In case of the peak at 1230 cm^{-1}, in the reverse scan, the initial value is not reached. For the peak at 1390 cm^{-1}, absorbance does, however, remain almost constant throughout the reverse

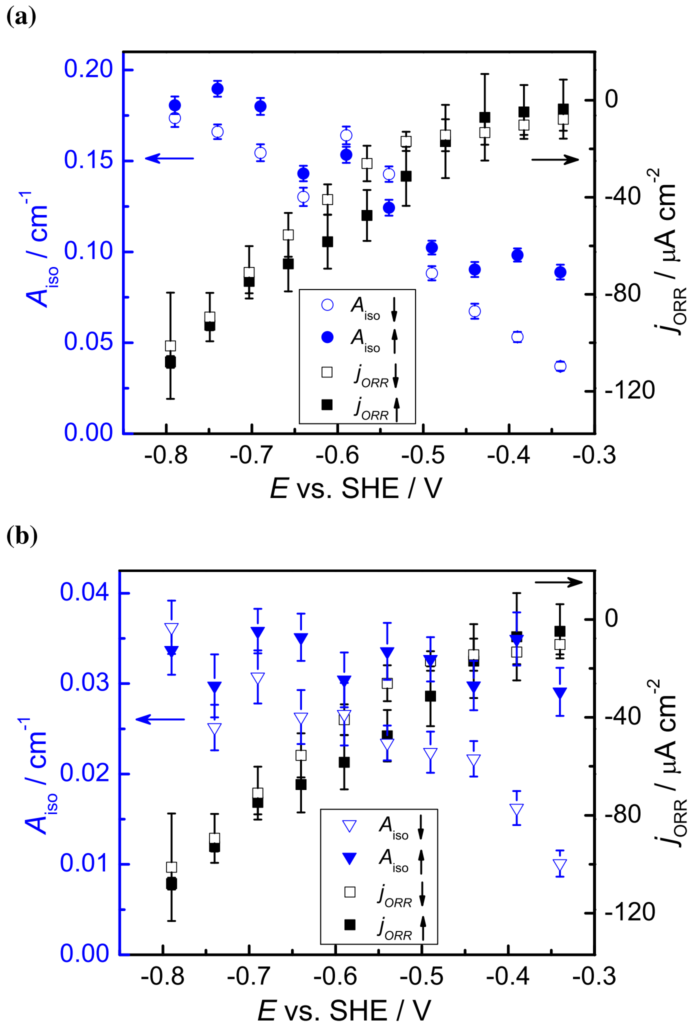

Figure 7 Comparison of potential dependence of ORR current densities with A_{iso} for (a) the absorption at 1230 cm^{-1} and (b) the absorption at 1390 cm^{-1} in 0.1 M NaCl at p*H* 10.5. Open symbols indicate scans in cathodic direction (↓), while filled symbols indicate scans in anodic direction (↑).

scan.

3.3. Experiments with isotope-labelled reagents

Experiments with isotope labelled species offer a way of arriving at a band assignment, or of validating a tentative assignment. The most prominent mode in the experimental spectra, centred around 1205 cm^{-1} (in $NaClO_4$) or 1230 cm^{-1} (in NaCl) should shift in frequency upon deuteration if it contains significant contributions due to motion of a hydrogen atom. To check that experimentally, experiments in D_2O-based electrolytes have been carried out. Unfortunately, the solvent's broad absorption due to the D-O-D bending mode makes an analysis of the spectrum around 1200 cm^{-1} impossible. In this region of the spectrum, peaks should appear which are not affected by the isotope exchange. The vibrational mode at $\sim$940 cm^{-1} appears unchanged in the spectra.

A second possibility of isotopic labelling in the study of ORR is using $^{18}O_2$ as O_2 source. An experiment with $^{18}O_2$ was carried out in 0.1 M NaCl electrolyte. Here, starting from an Ar-saturated electrolyte, the electrolyte was saturated with $^{18}O_2$ as described in section 2.3. Subsequently, IR spectra were recorded from -0.59 till -0.79 V in steps of 50 mV. All the spectra were referenced against the spectrum at -0.59 V in $^{18}O_2$. A comparison between the peaks at -0.79 V in $^{18}O_2$, and O_2 with natural isotope composition, consisting predominantly of $^{16}O_2$, is shown in Fig. 8. The band which is observed at $\sim$1230 cm^{-1} is shifting by $\sim$75 cm^{-1} to lower wavenumbers. Such a shift clearly shows the prominent involvement of O-atoms in the vibrational mode leading to this absorption. At the same time, peak position of the peak at 1390 cm^{-1} remains unchanged. The CVs using $^{18}O_2$ agree with CVs in O_2 with natural isotope composition within the error limits of these experiments. Currents between different experiments vary by $\sim$15 %, which is insufficient to study the kinetic isotope effect.

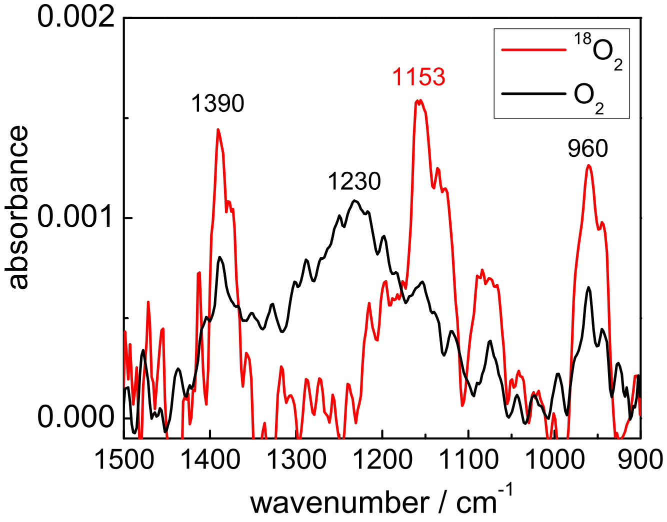

Figure 8 Comparison of ATR-IR spectra (p-polarisation) at -0.79 V in NaCl solution saturated with $^{18}O_2$ (—) and O_2 (—) with natural isotope composition.

4. Discussion

4.1. Interpretation of ATR-IR spectra

The assignment of the observed vibrational modes to the experimentally observed peaks in the spectra closely follows the line of reasoning presented elsewhere for spectra acquired under acidic conditions [16]. In particular, the results of vibrational frequencies and TDMs calculated for various structures using density functional theory were decisive in the assignments [16]. Final assignment of the peaks in the ATR-IR spectra, which will be discussed in the subsequent paragraphs, together with the corresponding θ are summarized in Table 1.

	superoxide	peroxide	Ge–OClO$_3$
	O–O str.	OOH bend	O–Cl str.
ClO_4^-	1205 cm^{-1}	1385 cm^{-1}	1025 cm^{-1}
	$(38 \pm 10)^\circ$	$(46 \pm 6)^\circ$	(not determined)
Cl^-	1230 cm^{-1}	1390 cm^{-1}	(not observed)
	$(43 \pm 5)^\circ$	$(40 \pm 10)^\circ$	(not observed)

Table 1 Summary of peak frequencies, assignments and tilt angle θ of the TDMs for the observed intermediates during ORR.

4.1.1. Peak at 1205 / 1230 cm^{-1}

The most prominent peak was observed at 1205 cm^{-1} in $NaClO_4$ and at 1230 cm^{-1} in NaCl based electrolyte. From the dichroic ratio, θ was determined to be $(38 \pm 10)^\circ$ in $NaClO_4$ and $(43 \pm 5)^\circ$ in NaCl. The corresponding mode in $HClO_4$ at 1210 cm^{-1} was assigned to an O–O stretching mode of surface–bound superoxide [16]. When using $^{18}O_2$ in NaCl, the peak shifts to 1153 cm^{-1} (Fig. 8). This result is in excellent agreement with the expected value for the isotope shift of a pure stretching mode when replacing $^{16}O_2$ with $^{18}O_2$, $1230\ \mathrm{cm}^{-1} \cdot \sqrt{\frac{16}{18}} = 1160\ \mathrm{cm}^{-1}$. The isotope shift confirms the assignment to an O–O stretching mode of superoxide also for the absorption observed in this work. As in both electrolytes studied here, the observed orientation of the TDM is nearly isotropic ($\theta_{\text{isotropic}} \simeq 54.6^\circ$), it is not immediately clear if there are species present which are not bound to the surface. However, for dissolved $O_2^{\bullet-}$, the solvation and temporal fluctuations cause a weak TDM, leading at maximum to a very weak IR absorption. Therefore, the absorption is very likely to be caused by surface bound superoxide, Ge–$O_2^{\bullet}$. The higher θ compared to the situation in $HClO_4$ is attributed to the difference in surface termination. In acidic solution, at the potentials where ORR occurs, the surface is H-terminated [16]. The

OH-terminated surface under alkaline conditions can act as H-bond donor and as H-bond acceptor, as opposed to the unpolar Ge–H bonds. This result is consistent with results from DFT calculations [16].

Comparing $HClO_4$ [16] and $NaClO_4$ shows a small shift of $\sim$5 cm^{-1} in peak frequencies. Remarkably, there is a significant shift of the peak centre of the superoxide mode comparing ClO_4^- and Cl^- electrolytes. This shift may be related to a difference in surface termination in the two electrolytes, and will be discussed in section 4.3.

In the initial spectra, when the electrode potential is stepped in negative direction, the potential-dependence of A_{iso} of this absorption closely follows j_{ORR} in both electrolytes. This result implies that the concentration of superoxide on the electrode surface increases with increasing net rate of the ORR – a result which is not surprising. As noted already in sections 3.1 and 3.2, in the reverse scans with increasing potential, A_{iso} in both electrolytes – though decreasing – does not reach its initial value, it remains at $\approx$1/3 of the maximum value in NaCl and $NaClO_4$. Such a result is in contrast to the behaviour observed in $HClO_4$ [16]. Two reasons can be the origin for this observed behaviour, (a) superoxo species residing on the surface for a rather long time, because further reduction is kinetically hindered or at least too slow to contribute to the current in a detectable manner, and (b) the presence of dissolved superoxide, which has moved too far from the electrode to undergo electron transfer from the surface but is still close enough to be detected by the evanescent wave. In both cases, the superoxo species which contribute to the absorption must be stable for minutes, though in general mobile superoxide is prone to dispropotionation according to $2\,O_2^{\bullet -} + H_2O \longrightarrow O_2 + HOO^- + OH^-$ [47, 48].

In $HClO_4$ [16], minor contributions of a surface-bound perchlorate to the superoxide peak around 1210 cm^{-1} have been found at very negative potentials. In $NaClO_4$, such a contribution can not be excluded (see Section 4.1.3). On the other hand, in NaCl, no contribution from electrolyte species are possible. Therefore, such an explanation for the lack of complete return to its initial value of A_{iso} can be excluded.

4.1.2. Peak at 1385 / 1390 cm^{-1}

This peak is assigned to an OOH bending mode of a peroxide species. A detailed discussion of the assignment was presented elsewhere [16]. The peak frequency is in good agreement with the peak frequency observed for this mode in H_2O_2, and is also almost the same as observed in $HClO_4$ [16]. There is only a small shift in peak frequency between the different electrolytes of $\sim 5\ \mathrm{cm}^{-1}$. For this vibrational mode, θ has been calculated as $(46 \pm 6)^\circ$ in $NaClO_4$ and $(40 \pm 10)^\circ$ in NaCl. As remarked in section 4.1.1, these values are relatively close to $\theta_{\mathrm{isotropic}}$. Hence, an unequivocal assignment to surface-bound peroxide based on the dichroism is not possible; peroxide in solution may contribute to the absorption, as this is IR active. The full width at half maximum of the band is $\sim$35 cm^{-1}, substantially smaller than the width of 150 cm^{-1} observed for concentrated H_2O_2 solutions [16]. The bending modes in the vibrational spectrum of separated, monomeric, matrix-isolated H_2O_2 molecules show up a characteristic doublet of peaks with a full with at half maximum of $\sim$2 cm^{-1} [49]. After association [49], or hydration [50], the related absorption consists of many sub-peaks, leading to a broad overall absorption in aqueous solutions of H_2O_2 [51]. While in solution, many conformers and solvation states lead to a broad bending mode absorption, a surface-bound peroxide should possess only a limited number of possible conformers and solvation states to contribute [16]. The observed small peak width is hence treated as an indication of the absence of dissolved H_2O_2,therefore, also as an indication that the peak is mainly originating from surface-bound species.

In both investigated electrolytes, this mode gradually increases in absorbance with decreasing potential, hence also with increasing j_{ORR}. In the reverse scan, with increasing potential, A_{iso} decreases only slightly in $NaClO_4$, while it remains almost constant in

NaCl. The same possible explanations as mentioned in section 4.1.1 are applicable here, too. A number of peroxide species may stay surface-bound, without further participation in electron transfer reactions. These species may nevertheless be subject to chemical decomposition at a certain rate, which in addition to electrochemical reduction diminishes the number of species on the surface. An alternative possibility is that H_2O_2 is formed as a product of the ORR in alkaline solution, and this H_2O_2 is desorbing and diffusing away from the surface once formed. In the latter case, however, an increase in A_{iso} is expected, in contrast to the observation that it stays constant in the reverse scan. However, H_2O_2 may subsequently decompose chemically [7]. While the formation of H_2O_2 as a product of the reaction cannot be excluded, the results presented here make it unlikely.

4.1.3. Peak at 1020 cm^{-1}

A peak at 1030 cm^{-1}, observed in acidic solution, was previously assigned to a ClO_4 stretching mode of surface-bound perchlorate (Ge–O–ClO_3) [16]. The absence of this peak in NaCl confirms this assignment.

4.1.4. Peaks between 920 and 980 cm^{-1}

Absorptions in this region are present in Ar and in O_2. Therefore, these modes are not related to the ORR. A peak at 960 cm^{-1} has previously been assigned to a Ge–O stretching mode [52]. The vibrational spectra of germanium-based glasses show absorption maxima around 900 cm^{-1}, with components at higher frequencies [53]. The higher frequency components are typically assigned to antisymmetric Ge–O–Ge stretching modes [53]. The peak frequency does not shift upon deuteration, consistent with this interpretation. Here, as these species are present on the surface, they are sensitive to the electrolyte and environment. The reason for the relatively large shifts of peak frequencies are still not clear.

4.2. Comments on the electrochemistry of Ge(100)

Most of the electrochemical data on Ge surfaces available in the literature has been obtained in acidic solution [33, 35–38], and data at moderate alkaline p*H* is not available. Therefore, a few comments should be made on the general electrochemistry of Ge observed under the alkaline conditions, even though this is not in the direct focus of this work, and raises a number of questions. The first observation is that upon scanning the potential in negative direction, in Ar-saturated $NaClO_4$ the potential at which the currents become cathodic is $\sim$-0.6 V (Fig. 2), which corresponds almost exactly to the potential under which HER becomes thermodynamically possible [54]. If the cathodic currents originate from HER, this implies almost a complete absence of an overpotential for the HER. A direct comparison to acidic solution is difficult because of the dominance in CVs of the change in surface termination. It needs to be emphasized that there are no Ge–H modes detected in this work, therefore the surfaces are free from Ge–H groups. A systematic study of the surface transformation by CVs at varying p*H* showed that the surface transformation is expected to occur $\sim$-1.3 V at p*H* 10.5. On the other hand, in NaCl at p*H* 10.5, there is a cathodic current observed even at potentials below -0.4 V (Fig. 5), which for thermodynamic reasons cannot originate from HER. The nature of this current is unclear. While there is the possibility of residual O_2 in the system, the curves are quite repeatable, which is not expected if the reduction of residual O_2 is responsible for the currents. A possible cathodic process is the reduction of a surface oxide, which is expected, however, only at lower potentials [54]. For acidic Cl^- electrolyte, the surface has been shown to be Ge–Cl terminated [32]. The reaction is p*H*-dependent, $\equiv\mathrm{Ge}-\mathrm{OH}+\mathrm{HCl}\longrightarrow\equiv\mathrm{Ge}-\mathrm{Cl}+\mathrm{H_2O}$ in acidic and $\equiv\mathrm{Ge}-\mathrm{OH}+\mathrm{Cl^-}\longrightarrow\equiv\mathrm{Ge}-\mathrm{Cl}+\mathrm{OH^-}$ in alkaline solution [32]. It is not clear where the equilibrium is at p*H* 10.5, but the surfaces in the different electrolytes may be differently terminated, contributing to the observed differences.

A second unusual observation is the fact that the anodic current peak observed around 0 V in both electrolytes investigated here is approximately twice as high in O_2-saturated electrolyte when compared to Ar-saturated electrolyte. The current peak may be attributed to the formation of an oxide. Intuitively, this observation points to a direct involvement of O_2 in the oxide formation process. Chemically, it is, however, hard to imagine a mechanism for this interaction.

Both observations show that there is plenty of open questions of the understanding of the electrochemical properties of Ge under alkaline conditions.

4.3. Implications for the reaction mechanism

Details of the kinetics of the ORR have been discussed numerous times, and are not the topic of this work. Here, it is worth noting that in the scans in negative direction, A_{iso} increases with decreasing E, and follows directly j_{ORR}. A_{iso} obtained in ATR geometry for a crystal with N reflections is proportional to the concentration c of absorbing species in the volume near the interface (including adsorbed species), in analogy to Lambert-Beer's law [46, 55, 56],

$$A_{\text{iso}} = \alpha' c = \alpha'' \Gamma, \tag{3}$$

with a constant of proportionality α'. An equivalent expression is valid for the surface concentration Γ of adsorbed species in the absence of dissolved species, with the proportionality constant α'' [46]. (As discussed in section 4.1.1 and 4.1.2, the peaks detected here are likely to originate from surface-bound species, so the second form of eq. 3 is the more relevant for this work.) Considering the absorbance from reaction intermediates, c (and likewise, Γ) must be treated as time averaged concentration $\langle c \rangle_t$,

$$\langle c \rangle_t = \frac{1}{T} \int_0^T c(t) \mathrm{d}t, \tag{4}$$

where the average is over the duration T of the acquisition of one spectrum. Here, $\langle c\rangle_t$ of both superoxide and peroxide in the region near the interface is found to increase with increasing j_{ORR}. It is hard to derive a detailed kinetic model from j_{ORR} alone, and cases exist in which several models are consistent with kinetic data [2].

For the general relation between A_{iso} of an intermediate and the current density, consider the simplest possible reaction scheme of two consecutive electron transfer reactions with a single intermediate, where all additional aspects like adsorption and diffusion are not considered:

$$B \xrightarrow[k_1]{\mathrm{e}^-} C \xrightarrow[k_2]{\mathrm{e}^-} D \tag{5}$$

In a simplified view of ORR with H_2O_2 as a product, B can be identified as oxygen, C as superoxide, and D as peroxide (if protonation steps are taken as significantly faster than the electron transfer steps). In kinetically controlled electrode reactions, in the limit of low surface coverages, surface concentrations of the different species enter the rate equations,

$$\begin{aligned}
\mathrm{d}[B]/\mathrm{d}t &= -k_1[B] && (6)\\
\mathrm{d}[C]/\mathrm{d}t &= k_1[B]-k_2[C] = -\mathrm{d}[B]/\mathrm{d}t - k_2[C] && (7)\\
\mathrm{d}[D]/\mathrm{d}t &= k_2[C]. && (8)
\end{aligned}$$

The resulting current density in this case is given as the sum of the rates of the two electron transfer reactions, i.e.

$$|j| = F(-\mathrm{d}[B]/\mathrm{d}t + \mathrm{d}[D]/\mathrm{d}t), \text{ i.e.} \tag{9}$$

$$|j| = F(k_1[B] + k_2[C]), \tag{10}$$

where F is the Faraday constant. Solving eq. 7 for $k_1[B]$ and substituting the result into eq. 10 yields

$$\frac{|j|}{F} = \frac{\mathrm{d}[C]}{\mathrm{d}t} + 2k_2[C]. \tag{11}$$

Using the approximation of a quasi-stationary state of an unstable intermediate $\left(\frac{\mathrm{d}[C]}{\mathrm{d}t} \approx 0\right)$, it directly follows

$$[C] \approx \frac{|j|}{2Fk_2}. \tag{12}$$

This discussion should not be limited to the quasi-stationary case. The ordinary differential equation 11 can be solved for the general case where j is time-dependent. A solution to eq. 11 for this general case is

$$[C](t) = \mathrm{e}^{-2k_2t}\left\{\frac{1}{F}\int \mathrm{e}^{2k_2t}|j(t)|\mathrm{d}t + X_0\right\}, \tag{13}$$

where X_0 is an integration constant. While in general, the integration involving $j(t)$ can be carried out numerically, j in this work behaves in good approximation time-independent: after the first 10 % of the time at a certain potential, j changes by $< 1\%$. During the initial 10 % of the spectra acquisition at the respective potential, the change in j is likely to originate from a substantial amount from capacitive currents, which are not related to the electron transfer reaction, hence should not be considered for kinetic analysis. Solving eq. 11 with a time-independent j yields the solution

$$[C](t) = \mathrm{e}^{-2k_2t}\left(\frac{|j|}{2Fk_2}\mathrm{e}^{2k_2t} + X_1\right), \tag{14}$$

with integration constant $X_1 = [C]_0 - |j|/2Fk_2$, as obtained from the initial condition $[C](0) = [C]_0$, with initial surface concentration $[C]_0$ from the intermediate. Therefore,

$$[C](t) = \mathrm{e}^{-2k_2t}\frac{|j|}{2Fk_2}\left(\mathrm{e}^{2k_2t} - 1\right) + [C]_0\mathrm{e}^{-2k_2t}. \tag{15}$$

From this solution, the time average $\langle[C]\rangle_t$ from eq. 4 can be evaluated, yielding

$$\langle[C]\rangle_t = \frac{\mathrm{e}^{-2k_2T}}{4k_2^2TF}\left(2k_2T\mathrm{e}^{2k_2T} - \mathrm{e}^{2k_2T} + 1\right)|j| + \left(\frac{1}{2k_2} - \frac{e^{-2k_2T}}{2k_2}\right)[C]_0. \tag{16}$$

Before discussing this equation in the context of the results obtained here, it needs to be clarified that $k_2(E)$ depends on the electrode potential. Unfortunately, the functional form of this dependence is model-dependent, and could in a simple form e.g. follow the Butler-Volmer form, [57]

$$k_2 = k_{2,0} e^{\gamma(E-E_{eq})}, \tag{17}$$

where the meaning of γ is discussed at length in electrochemical textbooks [57] and E_{eq} is the equilibrium potential of the reaction under study. Alternative relations exist [57]. The overall dependence of $[C](E,|j|(E))$ is therefore difficult to express in general terms.

Both the full solution, eq. 16, and the quasi-stationary approximation, eq. 12, show a relationship between $[C]$ and $|j|$ of the form $[C] = \beta(E)|j| + X_2$, where the function $\beta(E)$ depends on the level of approximation, and the constant X_2 vanishes in the quasi-stationary case and if $[C]_0 = 0$. Combined with eq. 3, this yields a relationship between the absorbance $A_{iso}^{(C)}$ of reaction intermediate C and j:

$$A_{iso}^{(C)} = \alpha''(\beta(E)|j| + X_2). \tag{18}$$

A similar relation is found in case step $C \underset{k_2}{\longrightarrow} D$ is not an electron transfer step. In eq. 11, the factor 2 has to be removed, with resulting equations of the same structure, just modified numerical factors.

For a further analysis, A_{iso} shall be considered as a function of both $|j|$ and E. For this purpose, the results shown in Fig. 4a and Fig. 7a are displayed in the form of A_{iso} vs. j_{ORR} in Fig. 9. It is tempting from these results to determine a value of k_2, using eq. 16 and eq. 17. To arrive at a physically sound value which can be interpreted as the rate of the reaction from superoxide to peroxide, is, however, prevented by a number of obstacles besides the model-dependence of eq. 17. The first obstacle concerns the constant of proportionality α''. An expression has been derived for adsorbed lipid bilayers [46]. The transformation from a volume concentration in Lambert Beer's law (eq. 3) to a surface concentration is for a bilayer system relatively easy, as the sampling volume can be defined as crystal area time layer thickness. For the ORR intermediates, the layer thickness is, however, hard to define here, and may be on the order of a bond length, a region where continuum electrodynamics is considered not valid any more [58]. Furthermore, no validated molar absorption coefficient is known for the surface-bound intermediate.

Nevertheless, under certain assumptions, the reaction in the two electrolytes investigated here can be compared. First, the limiting quasi-stationary form shall be used, eq. 12 (which is the limiting form for large t from eq. 16). Second, the assumption is reasonable that that α'' is the same in the two electrolytes, and that the form of $k_2(E)$ is the same in both electrolytes. In this case, $A_{\text{iso}}/|j| \propto 1/k_{2,0}$. From the data shown in Fig. 9, it follows that $k_{2,0}$ in NaCl is approximately 3 times the value of $k_{2,0}$ in $NaClO_4$.

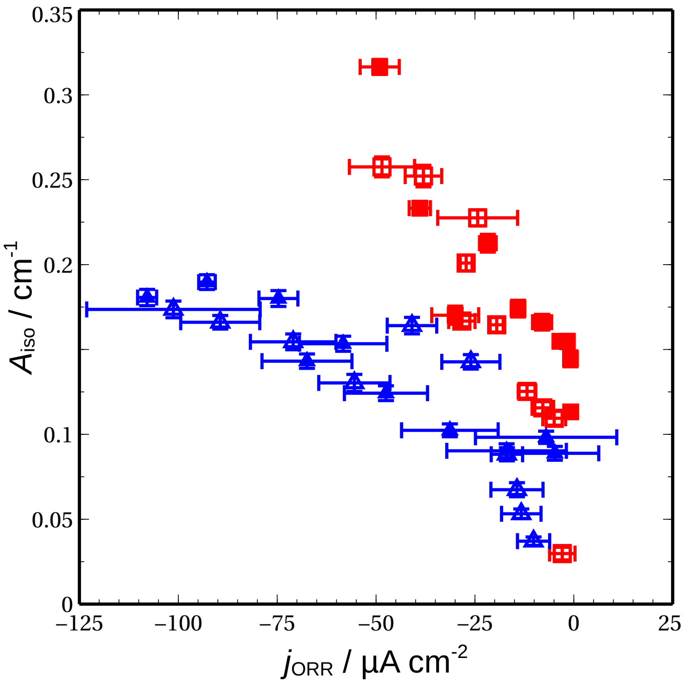

Figure 9 A_{iso} of the superoxide band vs. j_{ORR} in $NaClO_4$ (□ decreasing potential; ■ increasing potential) and NaCl (△ decreasing potential; ▲ increasing potential).

As a further complication, it must be noted that the full mechanism of the ORR is obviously more complicated than shown in the simple reaction scheme 5. The scheme should actually read

$$B \xrightarrow[k_1]{e^-} C \xrightarrow[k_2]{e^-} D \xrightarrow[k_3]{(e-)} \text{products} \tag{19}$$

More involved reaction schemes, mixtures of mechanisms, and non-electrochemical side reactions will inevitably also lead to expressions, which are consistent with the observations from this experiment, depending on the rate constants, diffusion rates, etc.. The authors would like to stress that also a simple generic reaction scheme as reaction 5 with one intermediate is sufficient to reproduce the main feature observed in the experiment here. The results for the simple scheme are valid for a small k_3.

The fact that A_{iso} is not completely decreasing to its initial value for both superoxide as well as peroxide in the reverse scan with increasing potential is in stark contrast to the behaviour in acidic solution [16]. As the currents return to zero in both cases, the results presented in this work indicate that especially in the reverse scan with increasing potentials, the absorption is in part due to products of the ORR with a lifetime exceeding the duration of an experiment, and not only due to intermediates. In other words, some intermediates are not further reduced and accumulate in the interfacial region. This accumulation is most pronounced in case of the peroxide (bending mode at 1390 cm^{-1}) in Cl^- electrolyte. Interestingly, in the reverse scans, the presence of these species does not result in a reduced rate of the ORR, as expected e.g. in case of a poisoning of active sites. Active sites must therefore be randomly generated on the Ge surface.

The increase with decreasing potential in absorbance of the mode at 940 cm^{-1} attributed to an antisymmetric stretching mode of bridging Ge–O–Ge [53], is initially counterintuitive. However, the species leading to the absorption may be surface bound OH^- on a hole in Ge, formed as a side product of the HER. The HER rate is increasing with decreasing potential, and is occurring in Ar-saturated as well as O_2-saturated electrolyte. This peak at 940 cm^{-1} is not observed at acidic pH [16], because of the higher stability of the Ge-H surface termination under acidic conditions. Its absence in $HClO_4$ may also be related to the different solubility of germanium oxides and hydroxides at different pH.

The most striking result in the IR spectra is the difference of 25 cm^{-1} in the vibrational frequencies of the surface-bound superoxide observed in the two electrolytes. Comparing the superoxide stretching frequency in $NaClO_4$ from this work with the corresponding frequency observed in $HClO_4$, only a small difference of 5 cm^{-1} is observed [16]. (A small effect of the electrolyte's anion on the frequency of the OOH bending mode of the peroxide intermediate is also visible.)

The first possible explanation for this observation is that actually, the observed absorption peaks are a superposition of several contributions. Using DFT calculations for perchlorate electrolyte, a contribution from surface-bound perchlorate has been identified on the low wavenumber side of the absorption peak [16]. This contribution is, however, paralleled by the observation of a second absorption peak $\sim$1030 cm^{-1}. In $HClO_4$, at several potentials, the peak attributed to superoxide is observed at $\sim$1210 cm^{-1} with no accompanying peak at 1030 cm^{-1}. This observation is treated as an indication that in perchlorate ($HClO_4$ and $NaClO_4$) electrolyte, the superposition with a perchlorate peak is not the reason for the observed difference of the peak positions when comparing to NaCl.

A second possible explanation starts from the fact that the vibrational frequency of O–O stretching modes is directly correlated with the bond order (see section 1) [15]. Therefore, the superoxide intermediate in Cl^- may have a higher bond order compared to the intermediate in ClO_4^-. At the same time, A_{iso} of the superoxide stretching mode in Cl^- is slightly lower than in ClO_4^-, and j_{ORR} in Cl^- is higher than in ClO_4^-. While in traditional electrochemistry, differences in reaction rates observed in supporting electrolytes with different anions are attributed to adsorption of the anion and the resulting blockage of active sites on the respective surface [59], the result from this work may be interpreted in a different direction. If the anion can affect the vibrational frequency of the intermediate, in at least one case in the investigated electrolytes, a presence of the anion in the vicinity (few Å) of the intermediate species is required. This result is equivalent to the formation of a anion-intermediate complex, which depends crucially on the nature of the anion. It should be pointed out that the Ge–$O_2^{\bullet}$ intermediate is charge-neutral, therefore no electrostatic repulsion between the anion and the intermediate occurs. The shift in vibrational frequency of the Ge–$O_2^{\bullet}$ intermediate with changing anion indicates an active involvement of the anion of the supporting electrolyte in the process of the ORR, stabilising or destabilising the intermediate in the reaction, with a direct consequence on the observed reaction rate and concentration of intermediates. The possibility of an essentially Ge–Cl terminated surface [32], or a mixed termination, as already mentioned in section 4.2, may provide an explanation for the interaction between Cl^- and the superoxide. Whether this is a special feature for Ge surfaces or is also occurring on other surfaces remains to be the topic of further investigation.

In acidic solution, a catalytic cycle was proposed as atomistic reaction model which proceeds via a surface radical, a superoxide and peroxide intermediate [16]. While the species detected in this work in alkaline solution are the same as reported before in acidic solution, there are significant differences in two respects, with consequences for the overall mechanism. First, in acidic solution, the onset of the ORR is correlated to a transformation in the surface termination to a Ge–H terminated surface, which also leads to a mechanistic coupling to the HER. At pH 10.5, HER and surface transformation are shifted to considerably more negative electrode potentials, while the ORR onset is only slightly shifted to more negative potentials. No Ge–H vibrational modes at ~ 2000 cm^{-1} are visible in the spectra in alkaline electrolytes, confirming the absence of Ge–H termination. As a result, the direct coupling to the HER is not obvious at alkaline pH, and the presence of radical intermediates on the surface has not been shown to the best of the author's knowledge.

However, a common feature between alkaline and acidic solution is the surface–bound superoxide intermediate. Second, the role of peroxide is different comparing acidic and alkaline conditions. Under alkaline conditions, there are indications that relatively stable peroxide species form during the ORR. On the other hand, in acidic solution, surface–bound peroxide was detected only at slightly negative electrode potentials, with absorbance decreasing with more negative electrode potentials [16]. The consequence is that a simple reaction scheme like reaction 5 is not sufficient to describe the behaviour of A_{iso} of the superoxide intermediate in relation to j_{ORR} in $HClO_4$.

5. Conclusions

The ORR on n-Ge(100) in alkaline solution proceeds via tilted surface-bound superoxide and peroxide, similar to results in $HClO_4$ [16]. As opposed to acidic conditions, significant amounts of peroxide are present at the electrode surface in alkaline solution. The difference in vibrational frequency of the surface-bound superoxide intermediate with changing anion in the electrolyte (Cl^- vs. ClO_4^-) may be interpreted as a hint that there is a direct involvement of the counterions in the stabilisation of ORR intermediates (not the transition state!). On the system investigated here, a Ge–Cl surface termination may provide an explanation for this observation: Cl^- is strongly adsorbed to the electrode surface, and hence always present in the vicinity of the superoxide intermediate forming on the surface. This concept needs a systematic study for different surfaces and most importantly electrolytes, as net rates will be affected by a change in stability of intermediates.

Detailed kinetic studies combining reflection spectroscopy and electrochemistry can in principle be used to unravel details of the reaction mechanism. From the data shown here, it is concluded that the second electron transfer step, i.e. the step from superoxide to peroxide, on n-Ge(100) is faster in NaCl than in $NaClO_4$. For more detailed studies, time-dependent measurements of the absorbance and an analysis using eq. 14 are needed, as in this way, rates of individual steps of the ORR can be directly obtained, and the relationship $k(E)$ can be experimentally mapped out. Such information is required for a molecular level understanding of the ORR.

Acknowledgements

S.N. acknowledges the International Max Planck Research School for Surface and Interface Engineering in Advanced Materials (IMPRS-SurMat) for a doctoral fellowship. P. U. B. thanks Thyssen Krupp Steel Europe for the funding of a collaborative research project. All authors thank MPIE workshop for the building of the in situ ATR-IR electrochemical cell used in this work.

References

[1] J. P. Hoare, The Electrochemistry of Oxygen, Interscience, New York, 1968.

[2] K. Kinoshita, Electrochemical Oxygen Technology, volume 1117 of *Electrochemical Society Series*, Wiley, New York, 1992.

[3] A. A. Gewirth, M. S. Thorum, Inorg. Chem. 49 (2010) 3557–3566.

[4] F. Cheng, J. Chen, Chem. Soc. Rev. 41 (2012) 2172–2192.

[5] I. E. L. Stephens, A. S. Bondarenko, U. Gronbjerg, J. Rossmeisl, I. Chorkendorff, Energy Environ. Sci. 5 (2012) 6744–6762.

[6] N. Ramaswamy, S. Mukerjee, Adv. Phys. Chem. 2012 (2012) 491604.

[7] I. Katsounaros, W. B. Schneider, J. C. Meier, U. Benedikt, P. U. Biedermann, A. A. Auer, K. J. J. Mayrhofer, Phys. Chem. Chem. Phys. 14 (2012) 7384–7391.

[8] J. W. Schultze, A. W. Hassel, Passivity of metals, alloys, and semiconductors, in: A. J. Bard, M. Stratmann, G. S. Frankel (Eds.), Encyclopedia of electrochemistry, volume 4 - corrosion and oxide films, Wiley-VCH, Weinheim, 2003, pp. 216–270.

[9] Y. Feng, A. Gago, L. Timperman, N. Alonso-Vante, Electrochim. Acta 56 (2011) 1009 – 1022.

[10] F. Jaouen, E. Proietti, M. Lefevre, R. Chenitz, J.-P. Dodelet, G. Wu, H. T. Chung, C. M. Johnston, P. Zelenay, Energy Environ. Sci. 4 (2011) 114–130.

[11] Z. Pilbáth, L. Sziráki, Electrochim. Acta 53 (2008) 3218 – 3230.

[12] H. Wroblowa, S. Qaderi, J. Electroanal. Chem. Interfacial Electrochem. 279 (1990) 231 – 242.

[13] Y. Miyata, S. Asakura, Corros. Sci. 44 (2002) 589 – 602.

[14] C. Pettenkofer, I. Pockrand, A. Otto, Surf. Sci. 135 (1983) 52–64.

[15] T. Itoh, T. Maeda, A. Kasuya, Faraday Discuss. 132 (2006) 95–109.

[16] S. Nayak, P. U. Biedermann, M. Stratmann, A. Erbe, Phys. Chem. Chem. Phys. 15 (2013) 5771–5781.

[17] T. Itoh, K. Abe, K. Dokko, M. Mohamedi, I. Uchida, A. Kasuya, J. Electrochem. Soc. 151 (2004) A2042–A2046.

[18] X. Li, A. A. Gewirth, J. Am. Chem. Soc. 127 (2005) 5252.

[19] J. Kim, A. A. Gewirth, J. Phys. Chem. B 110 (2006) 2565–2571.

[20] M. H. Shao, R. R. Adzic, J. Phys. Chem. B 109 (2005) 16563–16566.

[21] M. Shao, P. Liu, R. R. Adzic, J. Am. Chem. Soc. 128 (2006) 7408–7409.

[22] Y. Ayato, K. Kunimatsu, M. Osawa, T. Okadaa, J. Electrochem. Soc. 153 (2006) A203–A209.

[23] K. Kunimatsu, T. Yoda, D. A. Tryk, H. Uchida, M. Watanabe, Phys. Chem. Chem. Phys. 12 (2010) 621–629.

[24] G. Vasan, Y. Chen, A. Erbe, J. Phys. Chem. C 115 (2011) 3025–3033.

[25] G. Vasan, A. Erbe, Phys. Chem. Chem. Phys. 14 (2012) 14702–14709.

[26] J. Brooker, P. A. Christensen, A. Hamnett, R. He, Faraday Discuss. 94 (1992) 339–360.

[27] J. B. MacNaughton, L.-A. Naslund, T. Anniyev, H. Ogasawara, A. Nilsson, Phys. Chem. Chem. Phys. 12 (2010) 5712–5716.

[28] A. Gonchar, T. Risse, H.-J. Freund, L. Giordano, C. Di Valentin, G. Pacchioni, Angew. Chem., Int. Ed. 50 (2011) 2635–2638.

[29] P. Vassilev, M. T. M. Koper, J. Phys. Chem. C 111 (2007) 2607–2613.

[30] J. A. Keith, G. Jerkiewicz, T. Jacob, ChemPhysChem 11 (2010) 779–2794.

[31] W. Brattain, C. Garrett, Bell System Tech. J. 34 (1955) 129–176.

[32] S. R. Amy, Y. J. Chabal, Passivation and characterization of germanium surfaces, in: A. Dimoulas, E. Gusev, P. C. McIntyre, M. Heyns (Eds.), Springer series in advanced

microelectronics, Vol. 27 - Advanced gate stacks for high-mobility semiconductors, Springer, Wiesbaden, 2007, pp. 73–113.

[33] I. M. Huygens, K. Strubbe, J. Electrochem. Soc. 155 (2008) F49–F54.

[34] K. Bohnenkamp, H. Engell, Z. Elektrochemie 61 (1957) 1184–1196.

[35] R. Memming, G. Neumann, J. Electroanal. Chem. 21 (1969) 295–305.

[36] J.-N. Chazalviel, A. Belaïdi, M. Safi, F. Maroun, B. Erne, F. Ozanam, Electrochim. Acta 45 (2000) 3205–3211.

[37] F. Maroun, F. Ozanam, J.-N. Chazalviel, J. Phys. Chem. B 103 (1999) 5280–5288.

[38] F. Maroun, J.-N. Chazalviel, F. Ozanam, D. Lincot, J. Electroanal. Chem. 549 (2003) 161–163.

[39] A. Maurer, W. Mindt, H. Gerischer, Surf. Sci. 4 (1966) 431–439.

[40] H. Gerischer, W. Mindt, Surf. Sci. 4 (1966) 440–451.

[41] A. Erbe, R. J. Bushby, S. D. Evans, L. J. C. Jeuken, J. Phys. Chem. B 111 (2007) 3515–3524.

[42] A. Erbe, http://home.arcor.de/aerbe/en/prog/spectraltools.html, 2013.

[43] V. Tolstoy, I. Chernyshova, V. Skryshevsky, Handbook of infrared spectroscopy of ultrathin films, Wiley, 2003.

[44] E. Goormaghtigh, V. Raussens, J.-M. Ruysschaert, Biochim. Biophys. Acta, Biomembr. 1422 (1999) 105–185.

[45] N. Harrick, Internal Reflection Spectroscopy, Harrick Scientific, 1987.

[46] P. Wenzl, M. Fringeli, J. Goette, U. P. Fringeli, Langmuir 10 (1994) 4253–4264.

[47] D. Sawyer, M. Gibian, Tetrahedron 35 (1979) 1471–1481.

[48] D. Sawyer, J. Valentine, Acc. Chem. Res. 14 (1981) 393–400.

[49] M. Pettersson, S. Tuominen, M. Rsnen, J. Phys. Chem. A 101 (1997) 1166–1171.

[50] A. D. Kulkarni, R. K. Pathak, L. J. Bartolotti, J. Phys. Chem. A 109 (2005) 4583–4590.

[51] O. Bain, P. Giguere, Can. J. Chem. 33 (1955) 527–545.

[52] K. P. Ishida, P. R. Griffiths, Anal. Chem. 66 (1994) 522–530.

[53] A. M. Efimov, Optical Constants of Inorganic Glasses, 1995, year, pp. 96–102.

[54] M. Pourbaix, Atlas of electrochemical equilibria in aqueous solutions, National Association of Corrosion Engineers / Centre Belge d'Etude de la Corrosion CEBELCOR, Houston / Bruxelles, 1974.

[55] W. Hansen, Spectrochim. Acta 21 (1965) 815–833.

[56] N. Harrick, F. du Pré, Appl. Opt. 5 (1966) 1739–1743.

[57] C. M. A. Brett, A. M. O. Brett, Electrochemistry - Principles, Methods, and Applications, Oxford University Press, Oxford; New York; Tokyo, 1993.

[58] J. D. Jackson, Classical Electrodynamics, Wiley, New York; Chichester, 1998.

[59] M. Nesselberger, S. Ashton, J. C. Meier, I. Katsounaros, K. J. J. Mayrhofer, M. Arenz, J. Am. Chem. Soc. 133 (2011) 17428–17433.